nature portfolio

https://doi.org/10.1038/s41561-022-00901-w

Supplementary information

Dominant role of mineral dust in cirrus cloud formation revealed by global-scale measurements

In the format provided by the authors and unedited

Supplementary Information for

Global-scale measurements reveal cirrus clouds are seeded by mineral dust aerosol

Karl D. Froyd*, Pengfei Yu, Gregory P. Schill, Charles A. Brock, Agnieszka Kupc, Christina J. Williamson, Eric J. Jensen, Eric Ray, Karen H. Rosenlof, Huisheng Bian, Anton S. Darmenov, Peter R. Colarco, Glenn S. Diskin, ThaoPaul Bui, and Daniel M. Murphy

This PDF file includes:

- Discussion of mineral dust spatial and seasonal patterns observed during ATom
- Discussion of CESM/CARMA model biases on the interpretation of UT dust source apportionment
- Discussion of heterogeneous nucleation and dust as the dominant ice-nucleating particle (INP) type
- Summary of principal assumptions and limitations
- Figures S1-S13
- Table S1
- References

Discussion of mineral dust spatial and seasonal patterns observed during ATom

Principal features

Dust in the remote atmosphere retains some of the spatial heterogeneity of surface emissions (Fig. 2 and S2-S4). Dissipating dust plumes give rise to the strong regional gradients and patchiness apparent in the curtain plots. The strongest feature in the ATom data set is the North African dust plume, identified as the darkest regions in all Atlantic pressure-latitude plots. Across the ATom deployments dust mean mass concentrations measured inside the plume ranged from 14 to 122 μg std-m^{-3} for the reported size range, with significant variability within each plume. The plume latitude over the eastern Atlantic varied predictably with season. At the sample locations the plume extended up to ~4-5 km altitude during all seasons, above which a very strong gradient was common, where mass concentrations decreased by ~1-2 orders of magnitude over the next 1-2 km. Neither the ocean basin transects nor the vertical profile plots indicate an obvious connection between the strong North African plume and dust concentrations directly above in the upper troposphere (UT). However, zonal transport of the North African plume was extensive. Back trajectory analysis indicates that some dust enhancements over the Pacific basin were from North Africa, particularly during ATom1 (Aug, 2016) and ATom2 (Feb, 2017).

Outside well-defined plumes, the northern extra tropics had the highest UT dust mass concentrations, seasonally 0.046-2.5 μg std-m^{-3} within the mid-latitude band. Over the Pacific, both Asian and North African emissions provide strong seasonal contributions. Pacific UT dust levels often exceeded those over the Atlantic (ATom-2, -3, and -4). The minimum regional dust mass occurred in a latitude band of the tropical Pacific that shifted seasonally due to changes in meteorology, convective storm locations, and dust emissions. Above 6 km mean concentrations through these regions ranged from 0.0008 to 0.031 μg std-m^{-3} seasonally. Despite that low-latitude dust emission sources can strongly impact tropical latitudes (Fig. 1), the persistent lack of dust in the tropical Pacific during ATom is consistent with very efficient convective aerosol removal (e.g., Williamson et al., 2019; Kupc et al, 2021). The southern extra-tropics were always less dusty than northern extra-tropics, consistent with the weaker southern emission sources, but have strong seasonal variability during ATom (Fig. S12). Recent studies indicate the importance of high-latitude dust emissions for regional aerosol properties and mixed-phase clouds (Dagsson-Waldhauserova et al., 2019; Sanchez-Marroquin et al., 2020). UT dust averages of 0.025-0.23μg std-m^{-3} were observed at >60°N and above 6 km during ATom-1, -2, and -3. During ATom4 a regional transport event (see below) enhanced the dust regional average to 3.3 μg std-m^{-3}. It remains unclear whether this NH polar UT dust is due to vertical transport of the comparatively weak high-latitude emissions or poleward transport of low- and mid-latitude sources (Fig. S6). In the very remote SH polar UT, dust averages were 0.0007 and 0.0008 μg std-m^{-3} for ATom-2 and -4 but notably higher in austral winter and spring, 0.044 and 0.068 μg std-m^{-3} for ATom-1 and -3.

Dust lofted with biomass burning smoke

Mineral dust particles have been observed within biomass burning (BB) smoke plumes sampled at ground level and aloft (Cremean et al., 2016; Froyd et al., 2014). During ATom, some of the brief dust enhancements captured by the pressure-latitude plots correspond to biomass burning plumes (Schill et al., 2020). Likewise, the broad regional dust enhancement throughout the ATom3 (Oct, 2017) remote southern hemisphere correlates with widespread,

aged smoke (Schill et al., 2020). Typically, dust mass concentrations do not exceed ~1 μg std-m^{-3} inside smoke plumes, although levels vary widely with plume intensity and likely with fire source conditions. Neither model routinely captured these smoke-sourced dust enhancements. In general, strong BB plumes that loft smoke above the boundary layer may provide a direct route for dust into the free troposphere. This dust lofting mechanism is not well captured by current dust emission schemes and warrants further study of observational data sets.

Enhanced Asian dust event in the UT

A widespread UT dust event was observed at high latitudes during ATom4 sampling in spring, 2018 (Fig. S4). Enhanced dust up to several μg std-m^{-3} was observed at latitudes above about 55°N and from about 140-90° west longitude over three flights between Apr 27 and May 21. The enhanced UT dust mass is particularly evident in the north Polar and Pacific northern mid-latitude vertical profiles, which are nearly flat or inverted with altitude. Back trajectory analysis suggests the dust originated in central Asia. Both models captured the enhanced dust plume. Agreement with the measurements was best at the highest altitudes (>10 km), which were often near or above the cold-point tropopause. Both models underestimated the average dust mass (~1 μg std-m^{-3}) below 10 km.

Discussion of CESM/CARMA model biases on the interpretation of UT dust source apportionment

Differences in the source-specific contributions to UT dust (Fig. 3, Table 1) are subject to simulated transport biases that could potentially differ between emission sources. A direct method to determine model bias would be to compare model output to measurements of dust from various regions. However, a direct verification of sources regions is not possible because the instrumentation cannot reliably distinguish dust particles emitted from different sources. The general conclusion for this paper is that Asian dust makes a disproportionate contribution to cirrus-forming regions. For this conclusion, relative biases in the model between Asian and North African dust are more important than modeled absolute concentrations. In particular, the bias ratio must be lower than emissions-normalized UT dust contribution ratios in Table 1, column 6.

We estimate the potential relative bias by comparing the CESM/CARMA mean biases versus the aircraft measurements (Fig. S5) for UT regions with high Asian versus North African dust contributions. We choose the tropical Atlantic latitude band (see Fig 2) at altitudes >6 km to represent North African UT outflow, and the Pacific mid-latitudes and polar regions at >6 km for Asian UT outflow. We consider the ATom4 (May) and ATom1 (Aug) deployments to capture the largest seasonal contributions for those dust sources.

The mean (linear) biases across all ATom campaigns are 0.50 and 0.73 for Asian and North African outflow regions, respectively. The ratio of the linear biases (0.69) is <1, indicating that relative Asian UT contributions may be slightly underestimated. More importantly, this Asian-North African bias ratio is closer to 1 than the monthly ranges for emissions-normalized ratio of Asian to North African UT concentrations (1.8-18.3, Table 1 column 6) and much closer to 1 than the average ratio for all months (9.7).

Fig. 3 indicates that North African and Asian contributions to the UT are highest from about April through September. The mean biases for Asian and North African outflow regions are 0.40 and 1.09 during ATom4 (May), and 2.87 and 1.95 for ATom1 (Aug). The Asian/North

African bias ratios are 0.36 and 1.47 for May and Aug. These bias estimates indicate that the model underestimates the Asian dust UT contribution by x2.78 ($=0.36^{-1}$) relative to North Africa in May, and overestimates Asian dust by x1.47 in Aug.

Several important points are summarized from this estimation of CESM/CARMA model biasing that are relevant to the UT dust source apportionment analysis in Fig. 3 and Table 1.

1. The model does not show consistent biasing between Asian and North African dust contributions to the UT.
2. Asian UT dust can be either under- or over-estimated relative to North African dust, with the largest bias acting to underestimate Asian dust.
3. The magnitude of the relative source biases are all <x3.
4. The estimated bias ratios are smaller than the ratio of Asian-to-North African emissions-normalized UT dust concentration, 9.7 (Table 1, column 6).

This analysis supports that paper's conclusion that that Asian dust has significantly higher transport efficiency to cirrus-forming regions. Furthermore, we note that Wiacek et al. report a similar conclusion using an ensemble trajectory analysis of Asian and North African emissions."

Discussion of heterogeneous nucleation and dust as the dominant ice-nucleating particle (INP) type

We focus on deposition mode heterogeneous nucleation, where supersaturated water vapor can nucleate ice onto dry particles, rather than immersion freezing, where liquid water first condenses on dust particles, then freezes. Deposition nucleation is a simpler process and has a fairly direct and predictable impact on initial cirrus properties, i.e., fewer and larger ice crystals than produced by homogeneous freezing. In contrast, immersion freezing occurs in the complex environment of a convective system, and the process involves multiple activation steps. Although recent studies demonstrate a relationship between immersion INP and convective cirrus radiative properties (Hawker et al., 2021), in general the effect of dust-initiated ice on a convective system is buffered by many other processes, such that dust's role on cirrus coverage and initial microphysical properties – the objective of this study – is difficult to determine. Also, deposition is the only heterogeneous freezing mode available through much of the upper troposphere (and for most of the sampled air parcels) because temperatures are too cold for liquid water.

The cirrus analysis assumes that mineral dust is the dominant INP type in the upper troposphere. This approach is consistent with the conclusions of Cziczo et al. (2013), who observed dust as the most abundant cirrus INP during several cirrus events and also estimated that dust was the most abundant cirrus INP type globally. While a complete analysis of all potential INP concentrations is beyond the scope of this paper, we estimated relative INP contributions for several non-dust INP candidates to help justify limiting the paper's scope to mineral dust.

PALMS measurements of other potential INP types are typically more uncertain than mineral dust, and nearly all other types have poorly constrained deposition nucleation efficiencies. The relative abundances of sea-salt (Murphy et al., 2019), bioaerosol (Zawadawicz et al., 2019), and biogenic organic-rich particles (Wolf et al., 2020), combined with their preliminary ice nucleation efficiencies (Cziczo et al, 2013; Wolf et al., 2020; Wagner et al., 2018), suggest that these INP do not compete with mineral dust (<10% and typically <<1% of INP) in any broad ATom UT region (latitude bands from Fig 2). We cannot fully exclude all

INP candidates, for instance glassy organic-rich particles and crystalline ammonium sulfate, due to their unknown phase and nucleation efficiencies. While non-dust heterogeneous INP types may contribute to remote UT cirrus under certain conditions, mineral dust's influence is conclusive and extensive. A more complete analysis of non-dust INP in the remote UT is ongoing.

Summary of principal assumptions and limitations

The following is a summary of the principal assumptions and limitations in the paper's methodology and how these relate to the conclusions.

- The very low dust abundance in the remote UT is the principal challenge to accurate in-situ mineral dust concentration measurements using the current method. Although the measurement method can achieve exceptional limits of detection (Fig. S1), single samples can have large statistical uncertainty. However, the use of large sample sets, e.g., global or broad atmospheric regions (Fig. 2 and S2-S5), allows for meaningful model evaluation.
- Dust's role in cirrus formation depends on dust abundance (Fig. S13). Here we use in-situ dust measurements to drive the cirrus model, but generally, cloud formation studies rely on simulated dust. Simulated UT aerosol mass can be erroneous by orders of magnitude for large-scale models that have not been constrained by airborne measurements of dust or other surface-emitted aerosol. In particular, dust abundance at cirrus-forming altitudes is highly dependent on the treatment of aerosol removal by clouds and convection. Although the models employed here demonstrate increased skill with revised aerosol removal schemes (Fig. S5), the accurate representation of parameterized removal processes remains an ongoing effort for these and other global models.
- The analysis of UT dust source apportionment assumes that the revised CESM model simulates dust emissions and transport with similar accuracy across different dust source regions. The analysis presented in Supplementary Information demonstrates that the relative transport biases for two major NH sources (Asia and North Africa) are much smaller than the difference in their dust transport efficiencies to the UT. This validation case supports the principal conclusion that Asian dust has significantly higher transport efficiency to cirrus-forming regions than other NH emission sources.
- Ice nucleation depends very strongly on temperature (Fig. S9). Temperature in the cirrus model is determined by forward trajectories up to 10 days in time, plus perturbations to simulate gravity wave activity. Temperature uncertainty may render ice formation conditions and locations uncertain for individual trajectories. However, the ensemble of 1000's of trajectory cases generates robust conclusions regarding relative importance of dust heterogeneous nucleation versus homogeneous freezing of aqueous aerosol.
- The cirrus formation analysis assumes that remote UT dust aerosol nucleate ice with similar efficiency to dust samples in laboratory studies. Increasing or reducing dust nucleation activity does not necessarily translate into significant changes in the relative contribution of dust heterogeneous nucleation to cirrus formation. For instance, if UT dust activity is lower than assumed, yet dust still forms ice prior to homogeneous freezing of aqueous particles, the dust-formed cirrus fraction (Fig. 5a,c) would be only slightly

lower, and dust heterogeneous nucleation would still prevent cirrus with high ice concentrations (Fig 5b).

- The cirrus formation analysis also assumes that dust is the dominant INP in the remote UT. As described in the Supplementary Information, preliminary estimates and previous observations support this assumption. However, we cannot fully exclude all other INP candidates, particularly particles whose nucleation activity depends on phase in addition to composition. Were a non-dust heterogeneous INP type abundant and active enough to compete with dust nucleation, dust's role in cirrus formation (Fig. 5a,c) would be reduced. However, dust and the additional heterogeneous INP would combine to further suppress homogeneous freezing and the fraction of clouds with abundant small ice crystals (Fig. 5b).

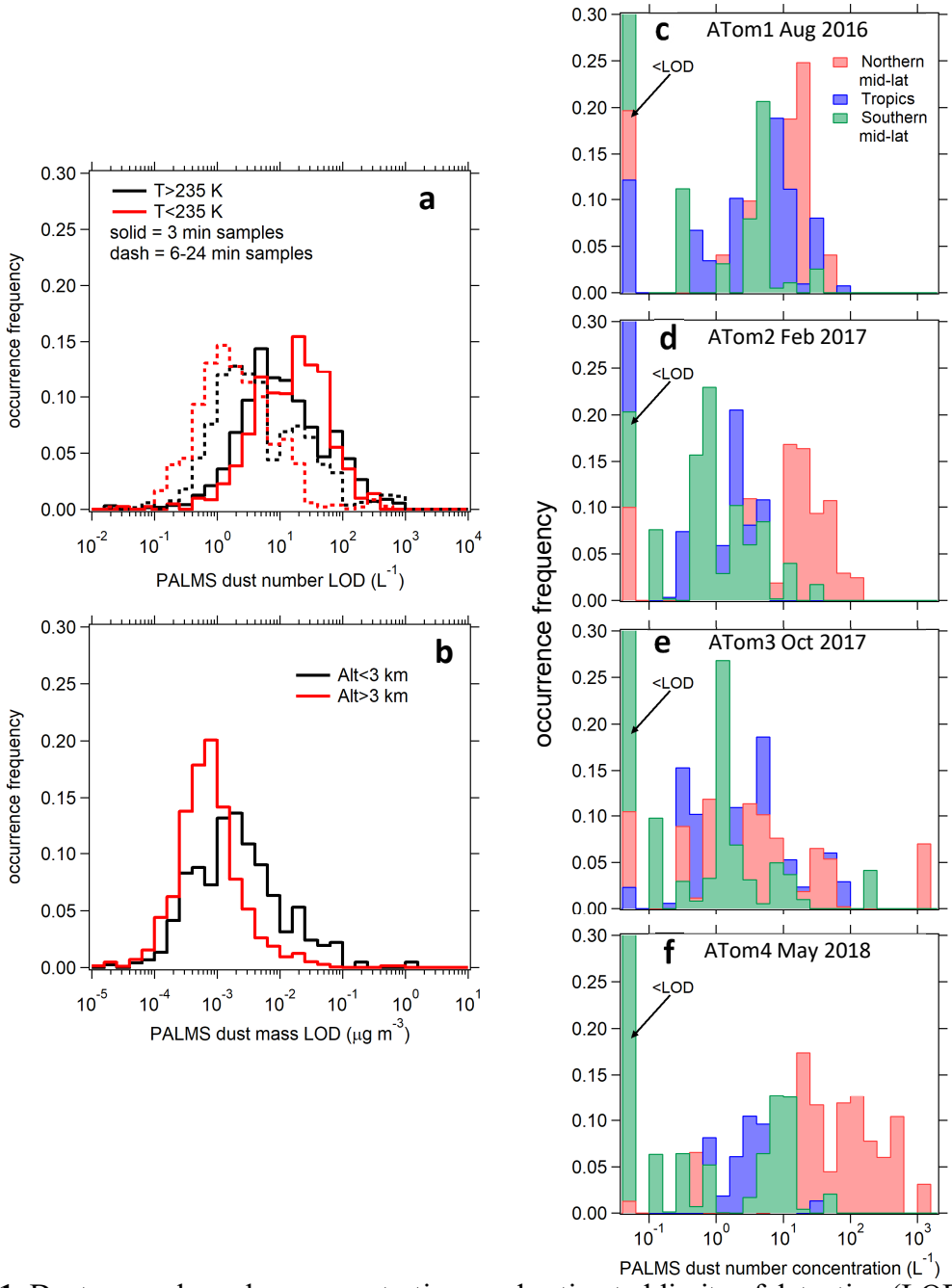

Fig. S1. Dust aerosol number concentrations and estimated limits of detection (LOD) from PALMS. LOD for every sample is plotted for a) number concentrations using two sample periods and for b) mass concentrations for 3 min samples during ATom1. To improve measurement sensitivity for the cirrus microphysical modeling analysis, longer time averages of 6-24 mins were used to calculate dust number concentrations (see Methods). The fraction of samples above LOD improved from 18% at 3 min to 75% with 6-24 min sample times. Typical number and mass LODs in the UT are ~0.5-10 L^{-1} and ~0.0001-0.01 μg m^{-3}, respectively. The high sensitivity of this technique enables measurements at concentrations relevant to UT cirrus ice particles, N_i ~10-1000 L^{-1}. c,d,f) Dust number concentrations in cirrus-forming regions (T<235 K) are plotted for all ATom campaigns.

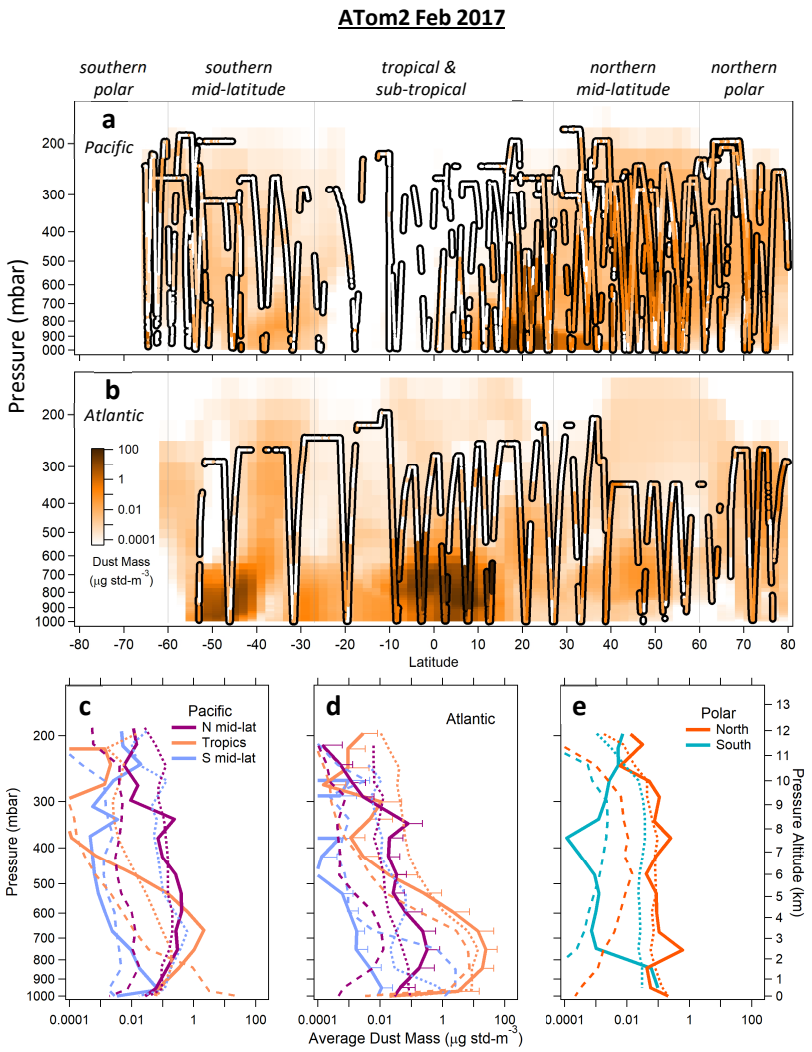

Fig. S2. Dust aerosol measurements and simulations during ATom2. Graphs are equivalent to Fig. 2. PALMS airborne mass spectrometer measurements over the Pacific basin (a,c), Atlantic basin (b,d), and polar regions for all longitudes (e) are compared to two models. Flight tracks (top panels) are colored by measured dust mass concentration on a log scale. The background shading shows simulated CESM/CARMA dust concentrations, plotted as vertical curtains at the aircraft location. Lines designate five latitude bands. In the lower panels, measured dust concentrations (solid) are compared to the CESM/CARMA (long dash) and GEOS/GOCART (short dash) simulations for each latitude band. Panel (d) shows representative standard deviations as error bars.

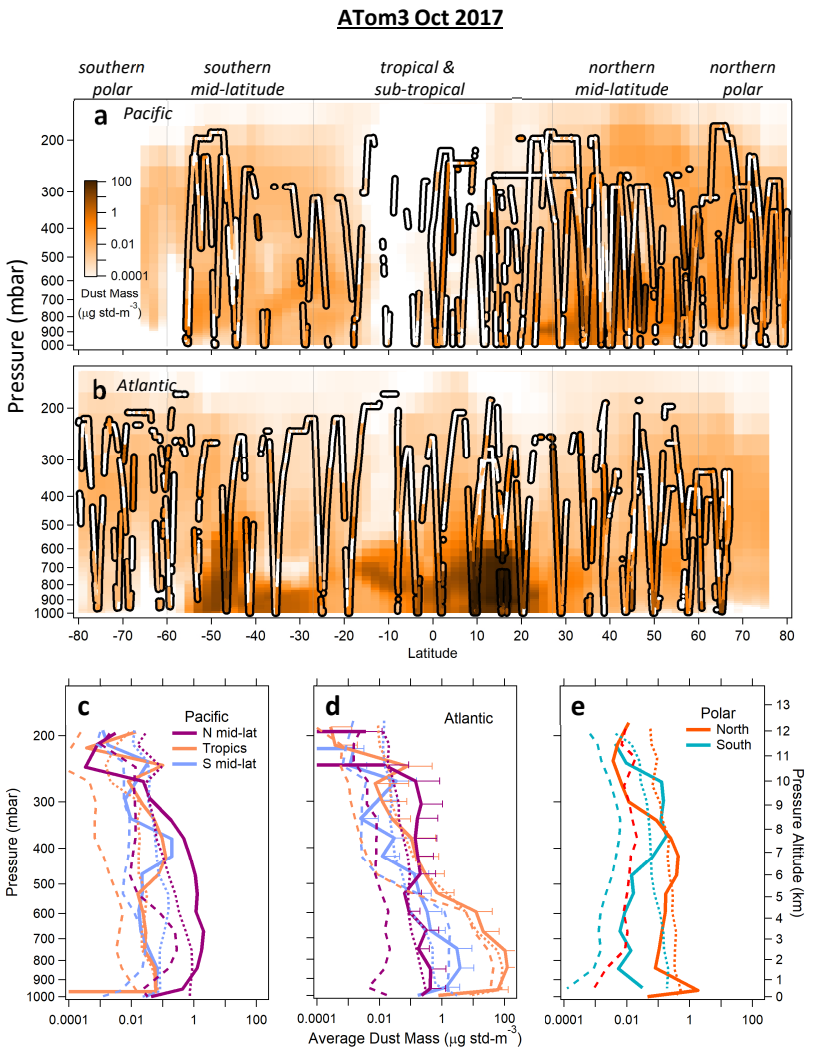

Fig. S3.
Graphs as in Fig S2 for ATom3 flights.

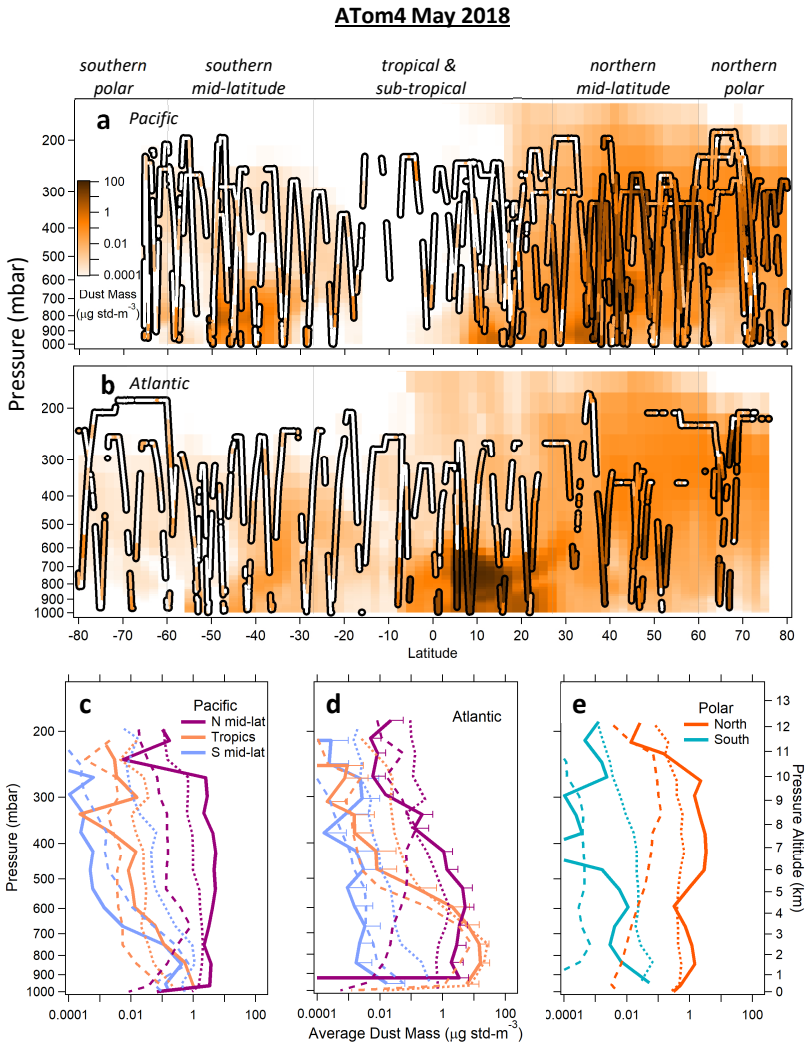

Fig. S4.
Graphs as in Fig S2 for ATom4 flights.

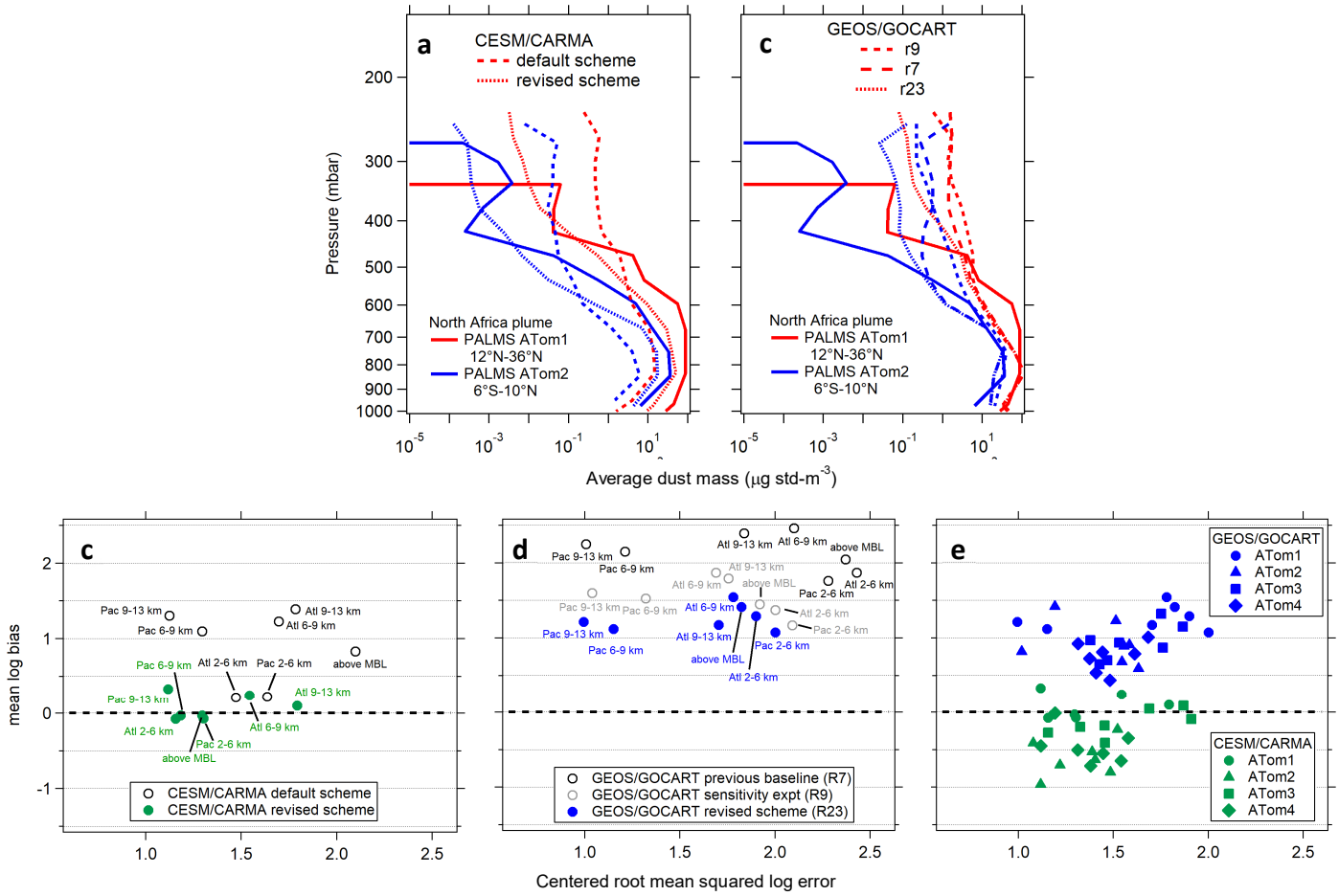

Fig. S5.

Evaluating dust aerosol in global models (see Methods for details). The default aerosol removal schemes in CESM/CARMA (a) and GEOS/GOCART (b) were recently revised (Yu et al., 2019; Schill et al, 2020; Bian et al., 2019), guided by measurements of surface-emitted aerosol during ATom. In this representative example the revised aerosol schemes reduced simulated dust aerosol by orders of magnitude in the UT, and agreement with ATom measurements is improved. Bias and variance for ATom1 dust mass concentrations in the CESM/CARMA model (c) and in the GEOS/GOCART model (d) are plotted for different altitude ranges and ocean basins and for all regions above the MBL. Prior to revision of aerosol convective transport schemes (open points), both models had high biases of >x10 (log bias >1) above the MBL in many regions, particularly at altitudes >6 km. The biases are reduced in both revised schemes (solid points). Panel (e) shows revised modeling results for all regions across all ATom deployments. For CESM/CARMA, mean linear biases in the majority of these broad regions are within a factor of 2 (mean log bias <|x0.3|) for altitudes >6 km.

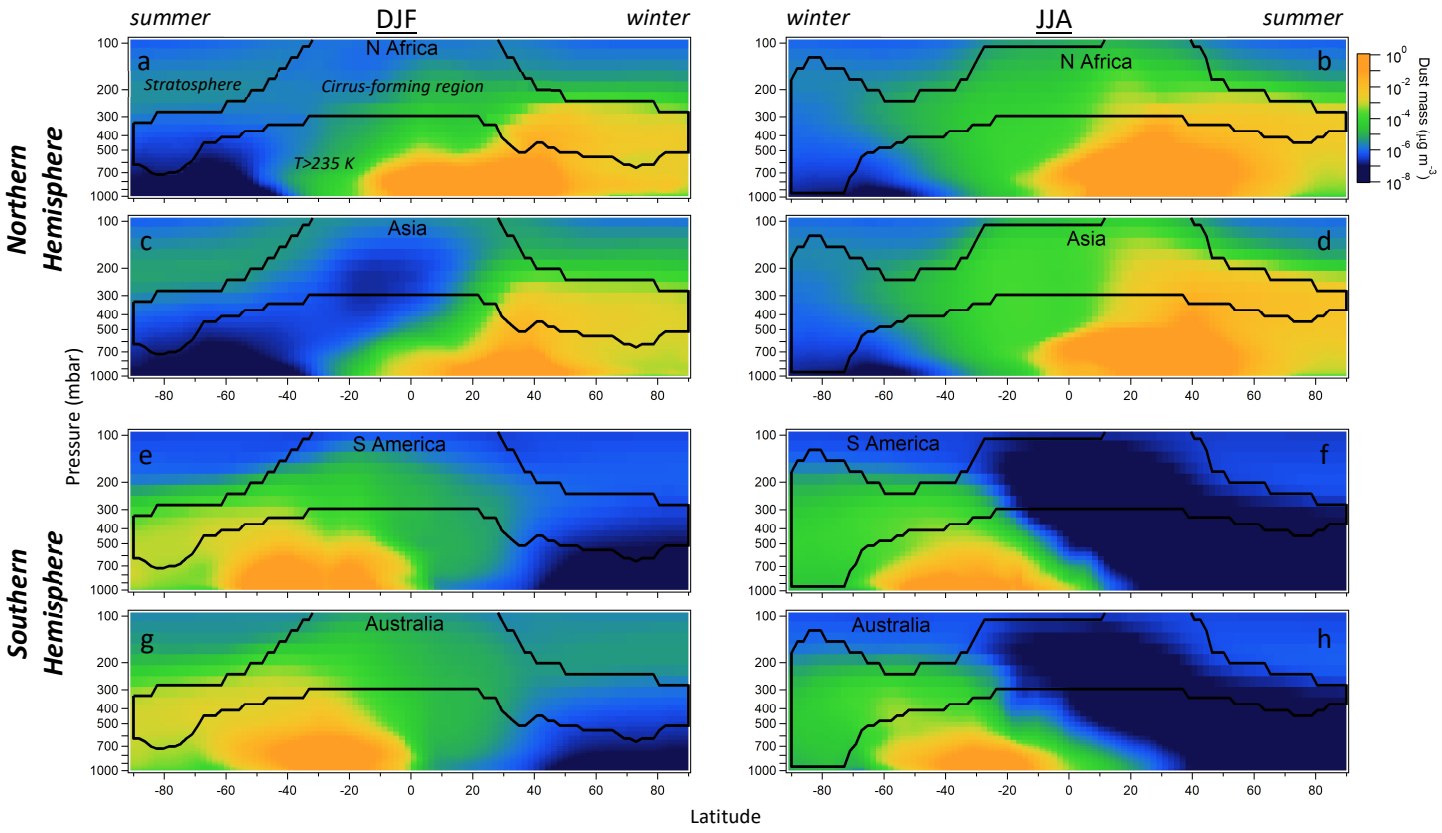

Fig. S6.

Mineral dust lofted into cirrus-forming regions from CESM/CARMA simulations. Contributions from the largest two emission zones in the NH (a,b,c,d) and SH (e,f,g,h) are colored by dust mass concentrations zonally averaged for two seasons, DJF and JJA, 2014-2018. Black lines enclose cirrus-forming regions, defined as T<235 K and below the cold point tropopause. Minimum altitudes for cirrus regions vary: tropical air must reach >10 km, whereas in polar latitudes deposition nucleation can occur near the surface during winter. Strong N-S gradients (~x100-1000) across the tropics indicate inefficient inter-hemispheric transport at high altitudes. Nevertheless, during boreal summer months intense NH emissions and deep convection combine to contribute 19-57% of the SH UT dust. Dust from low- and mid-latitude sources pools in the polar UT, where it may compete with contributions from high-latitude emissions (Bullard et al., 2016; Tobo et al., 2019; Sanchez-Marroquin et al., 2020).

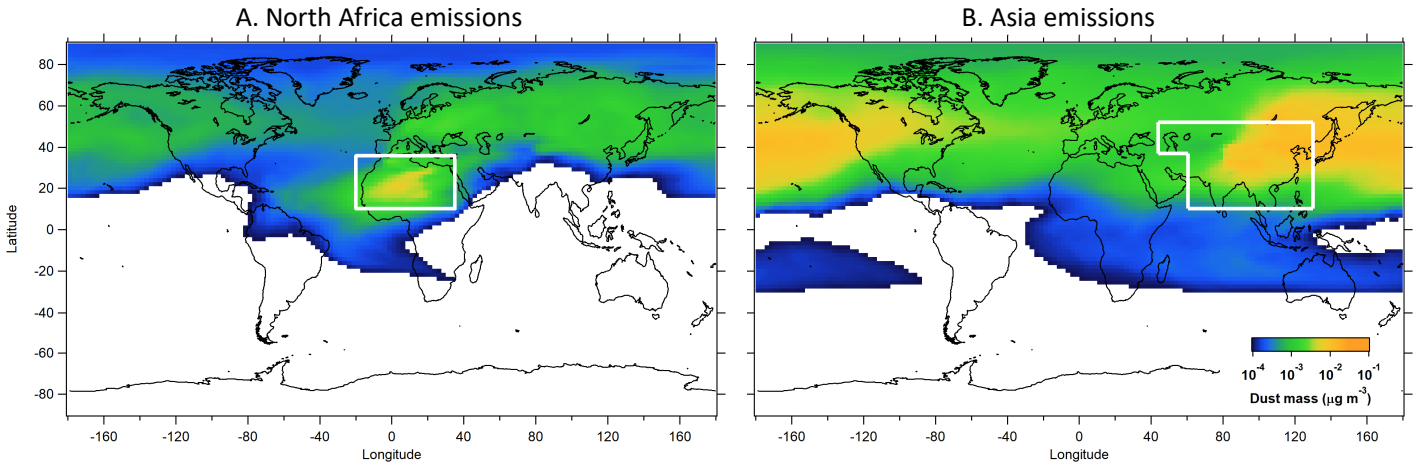

Fig. S7.

An example of vertical transport efficiency for dust emitted from (a) North Africa and (b) Asia simulated using CESM/CARMA for 2014-2018. Maps are colored by dust mass concentration averaged over 200-250 mbar in the upper troposphere for boreal summer months (JJA) when annual emissions are at their maxima. White boxes bound the emission zones from Fig. 1. Although Asia emits only one quarter the dust mass of North Africa during JJA, Asian emissions are more efficiently lofted to the UT. In particular, North African dust encounters less convection once leaving the African continent.

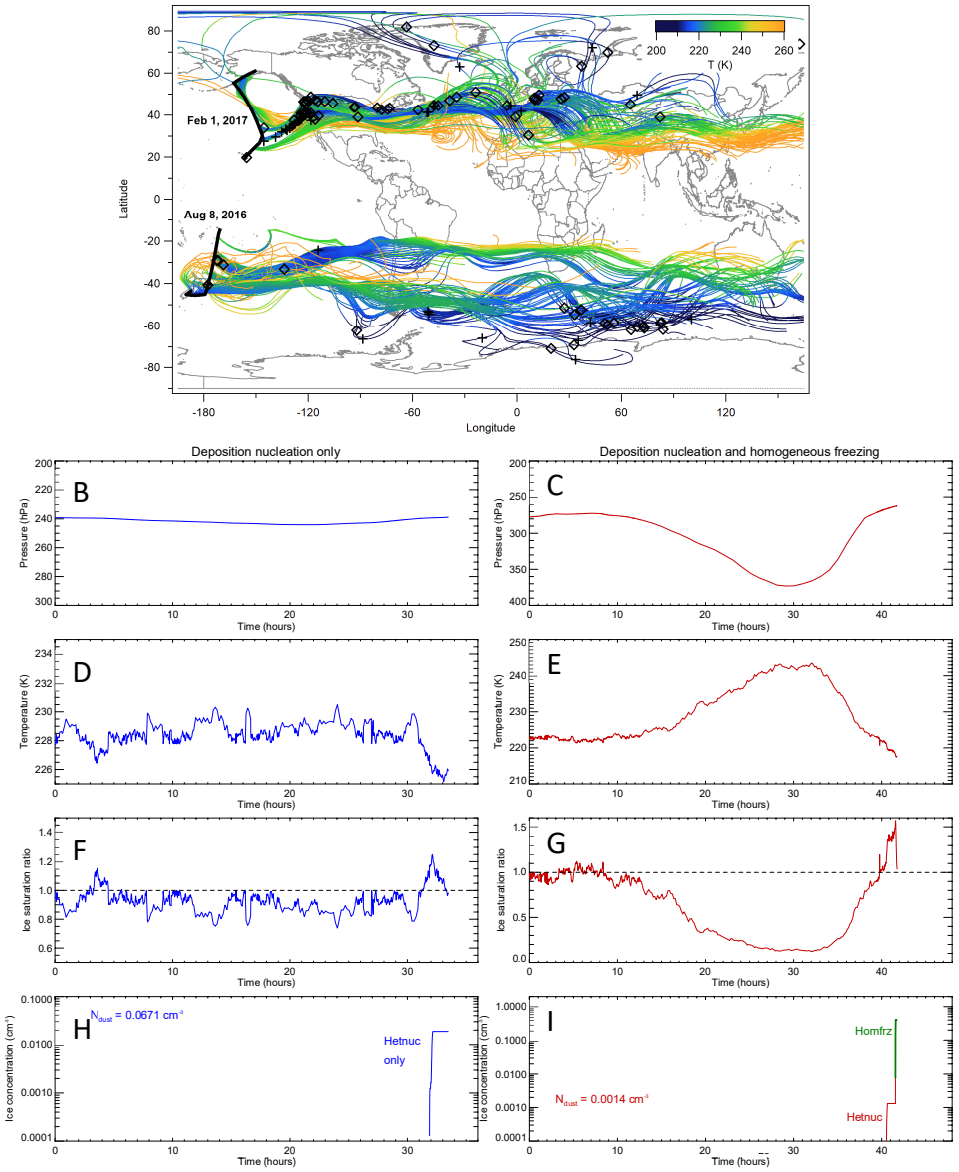

Fig. S8. Details of microphysical simulations of cirrus formation. a) Ten-day forward trajectories are initiated for every 1 min of flight time, shown for the ATom1 flight on Aug 8, 2016 and ATom2 flight on Feb 1, 2017. Colors indicate the evolving air temperature as air parcels ascend or descend. Black markers denote cirrus formed by heterogeneous nucleation on dust aerosol (diamonds) or homogeneous freezing of solution aerosol (crosses). b-i) Simulations of cirrus formation along two example forward trajectories are plotted as time series over several days. Air parcel temperatures (d,e) are defined by forward trajectories and also incorporate high-frequency perturbations to simulate gravity waves. When the ice saturation ratio (f) increases beyond the nucleation threshold for mineral dust, ice is formed (h). Rapidly growing ice crystals sequester the available water vapor, which can suppress further freezing events. However, if cooling occurs rapidly relative to water vapor deposition onto the new crystals, S_{ice} continues to increase above ~1.6 where homogeneous freezing then occurs, forming additional ice crystals (g,i), in which case both mechanisms contributed to the new cirrus cloud. The dominant mechanism is defined as that producing greater ice crystals.

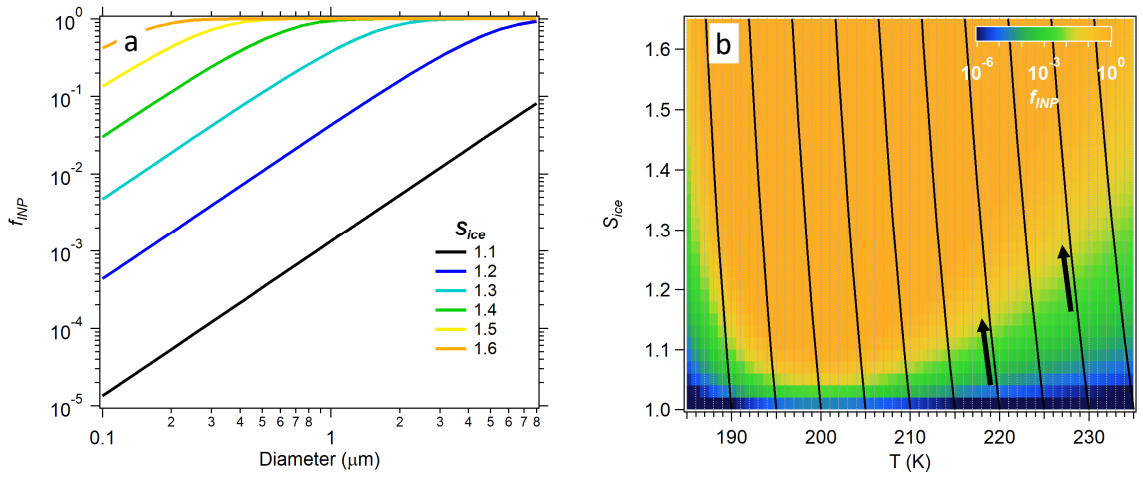

Fig. S9.
The fraction of dust particles that nucleate ice (f_{INP}) under ambient conditions is a very steep function of particle size, temperature, and S_{ice} (Ullrich et al., 2017). a) f_{INP} increases with particle surface area at 220 K. For example, 2 μm dust particles are x10 more active as INP than 0.8 μm particles. b) Air parcels cooled by large-scale ascent and gravity waves follow isolines of constant water vapor (black lines). Supersaturation is a strong function of temperature: a 1° cooling (arrows) can increase dust nucleation efficiency (colors) by several orders of magnitude. The cirrus nucleation model incorporates these strong dependencies.

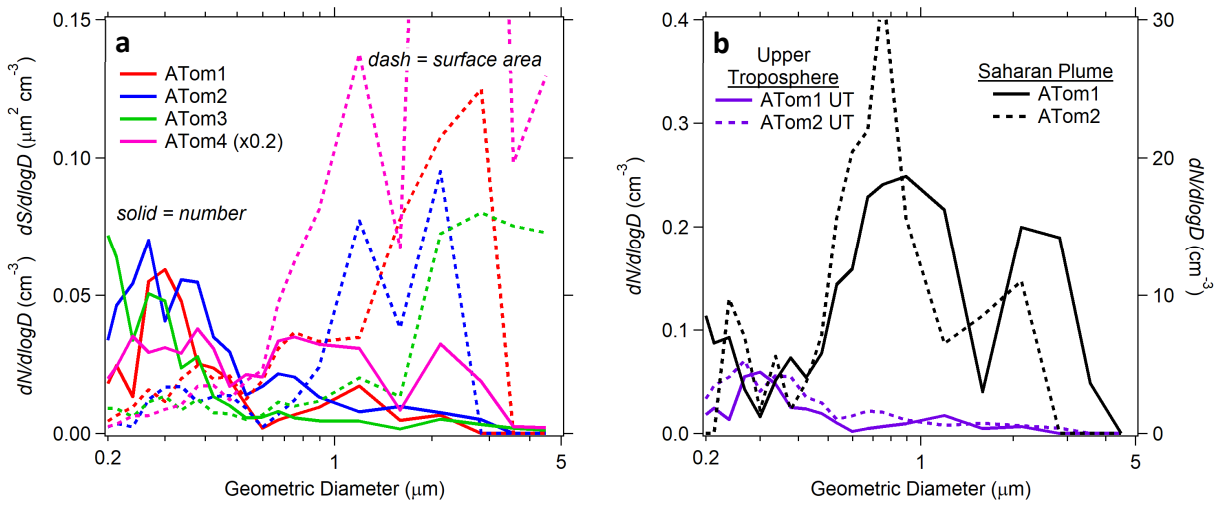

Fig. S10.

Average number and surface area size distributions for mineral dust particles in cirrus-forming regions measured by PALMS and size spectrometers. a) Submicron particles constitute about 20-40% of the dust surface area. Sizes smaller than 0.2 μm have negligible surface area. For simulations of cirrus formation, these campaign-averaged size distributions are scaled so that the total dust number concentration matches the number concentration measured in each sample. This approximation is necessary because, due to the low dust concentrations in the UT, the entire dust size distribution is not measured for every sample. b) The same number concentration data for ATom1 and ATom2 (left axis) are compared to samples taken within intense Saharan dust plumes at altitudes of 1 to 6.5 km over the Atlantic Ocean (right axis). Compared to the Saharan plume size distribution, larger upper tropospheric dust particles (D>0.5 μm) are depleted by factors of x12-15 relative to smaller particles.

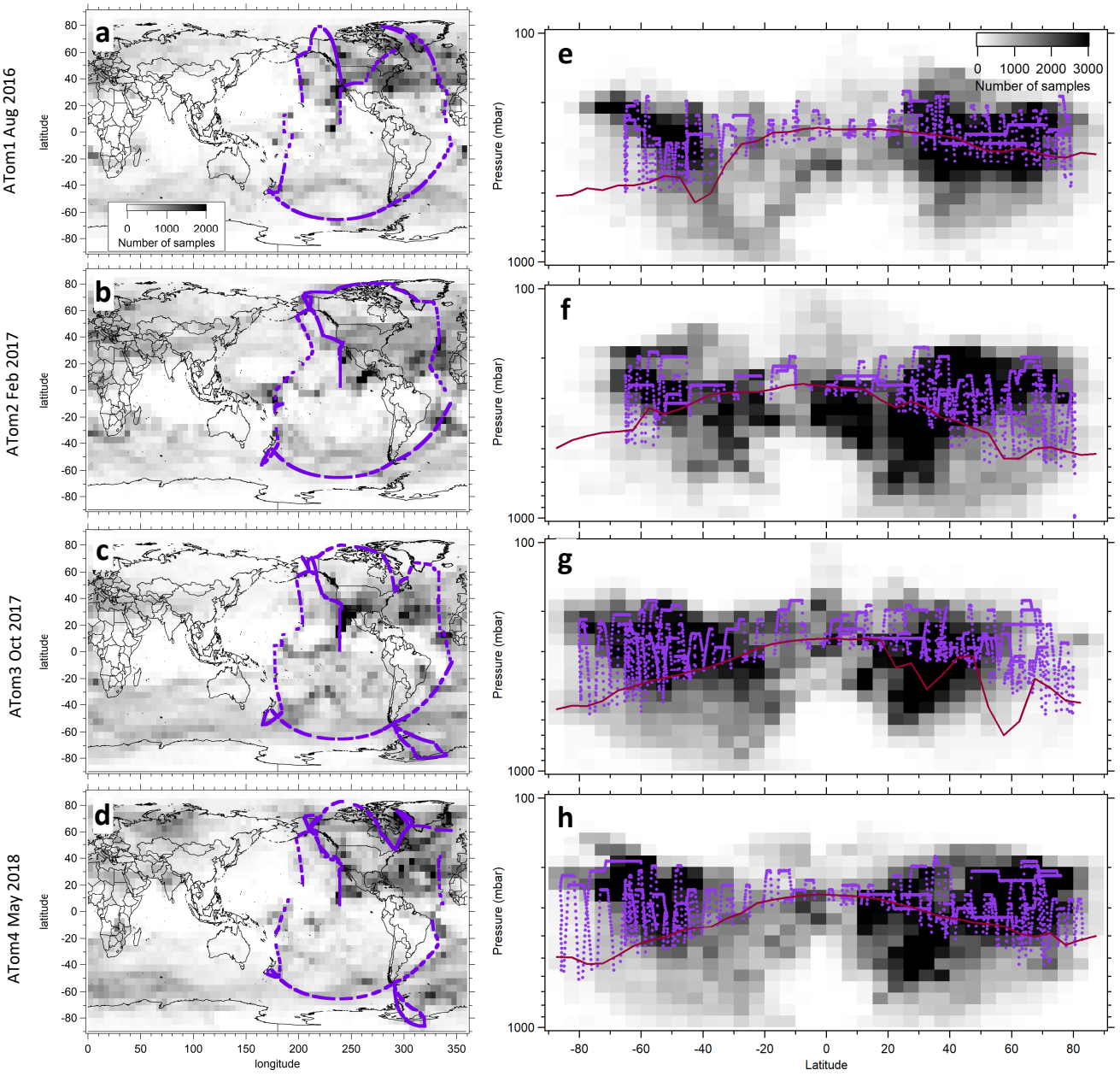

Fig. S11. Ten-day forward trajectories initiated at aircraft locations sample a large fraction of the globe. One-degree grid boxes are shaded by the number of 1-hr samples from all calculated trajectories (a-d). We restrict the geographic analysis primarily to latitude-altitude comparisons (e-h) since air parcels tend to stay within latitude ranges as they move zonally around the globe. The red line denotes the average pressure level above which cirrus can form by water vapor deposition (T<235 K). Tropical, mid-latitude, and polar regions are all sampled by 1000's of points. The TTL between 200 mbar and the tropopause is under-sampled, and consequently, this analysis cannot determine the relative importance of dust nucleation there. Trajectory starting locations at the aircraft position are plotted as purple dots.

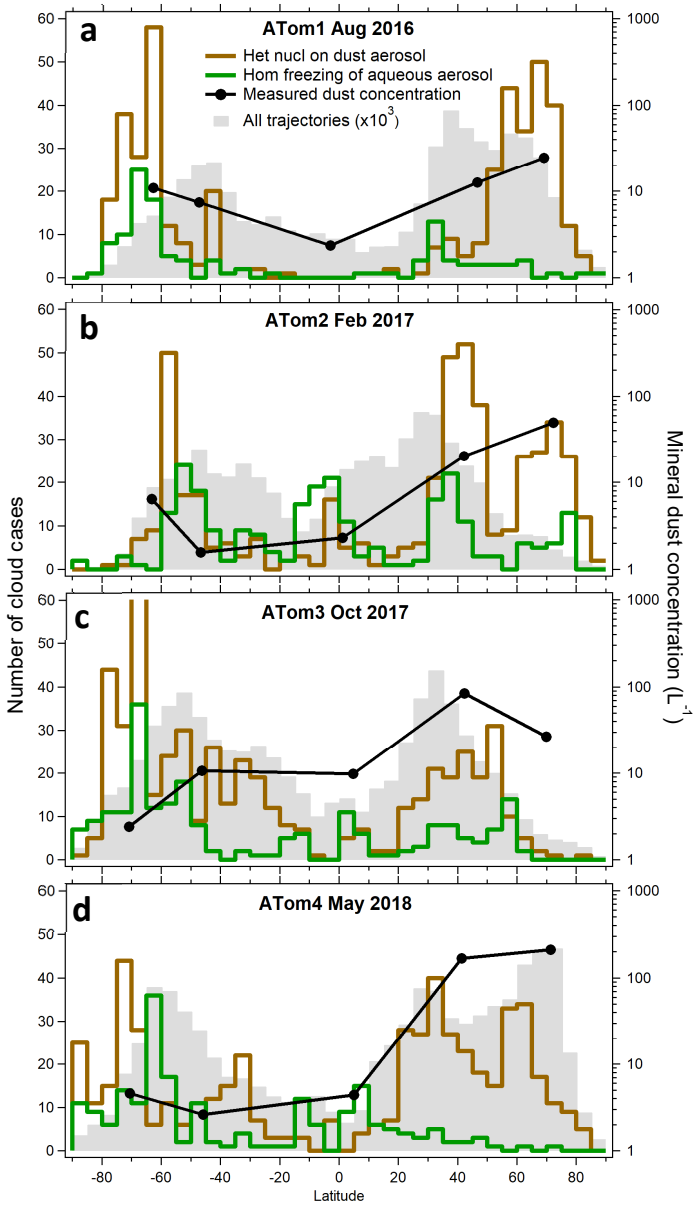

Fig. S12.
The seasonality of the cirrus formation mechanisms. Graph format is the same as Fig. 5.

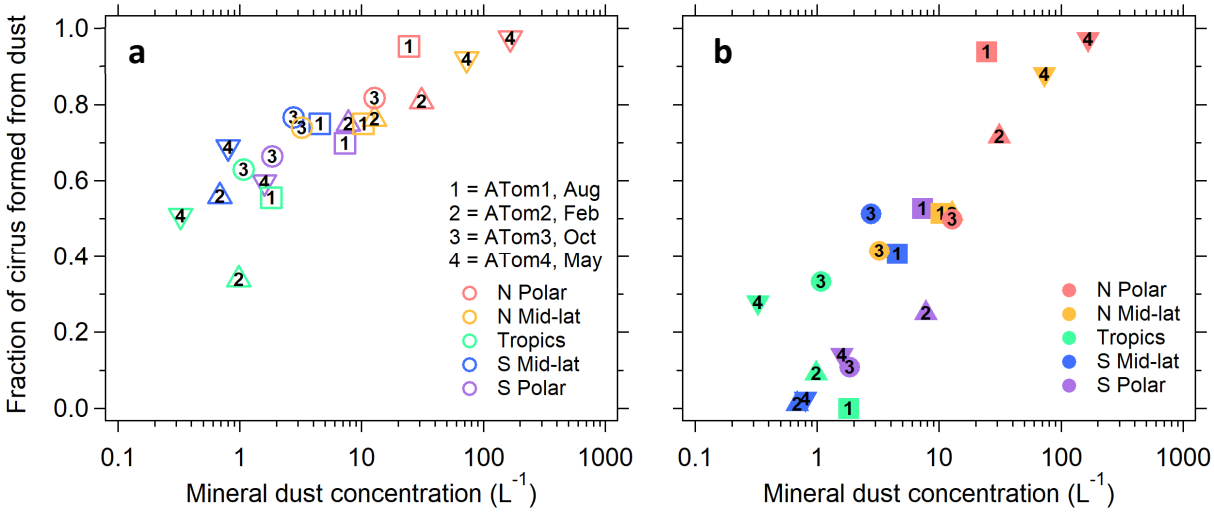

Fig. S13.

The cirrus formation mechanism depends principally on dust aerosol concentration. Median dust values for five latitude bands (colors) are plotted for all ATom seasonal deployments (symbols and numbers). Individual samples having concentrations below the measurement LOD were given half the LOD value. a) All cirrus cases, b) cirrus with ice concentrations N_i>10 L^{-1}.

Table S1.

GEOS wet scavenging treatments for the revised R23 compared to the R7 previous baseline case and the R9 sensitivity experiment.

Model parameter	R7 previous baseline	R9 sensitivity experiment	R23 revised scheme
f(large-scale-cloud)[a]	0.3	0.8	0.3
f(convective-scale-cloud)[a]	1.0	0.2	1.0
cold-cloud scavenging	no	no	yes

[a] f: precipitation scavenging coefficient

References

Bian, H. *et al.* Observationally constrained analysis of sea salt aerosol in the marine atmosphere. *Atmos. Chem. Phys.* **19**, 10773–10785 (2019).

Bullard, J. E. *et al.* High-latitude dust in the Earth system. *Rev. Geophys.* **54**, 447–485 (2016).

Creamean, J. M. *et al.* Colorado air quality impacted by long-range-transported aerosol: A set of case studies during the 2015 Pacific Northwest fires. *Atmos. Chem. Phys.* **16**, 12329–12345 (2016).

Cziczo, D. J. *et al.* Clarifying the dominant sources and mechanisms of cirrus cloud formation. *Science* **340**, 1320–4 (2013)

Dagsson-Waldhauserova, P. et al. Vertical distribution of aerosols in dust storms during the Arctic winter. *Sci. Rep*. 9, **16122** (2019).

Froyd, K. D., Liao, J., Murphy, D.M., Ziemba, L.D., Anderson, B.E., and Woods, S., Biomass Burning as a Source of Mineral Dust and Giant Aerosol to the Free Troposphere, *AGU Fall Meeting Abstracts* **2014**, A52A-04 (2014).

Hawker, R. E. *et al.* The temperature dependence of ice-nucleating particle concentrations affects the radiative properties of tropical convective cloud systems. *Atmos. Chem. Phys.* **21**, 5439–5461 (2021).

Kupc, A. *et al.* The potential role of organics in new particle formation and initial growth in the remote tropical upper troposphere. *Atmos Chem Phys* **20**, 15037–15060 (2020) doi:10.5194/acp-20-15037-2020.

Murphy, D. M. *et al.* The distribution of sea-salt aerosol in the global troposphere. *Atmos. Chem. Phys.* **19**, 4093–4104 (2019).

Sanchez-Marroquin, A. *et al.* Iceland is an episodic source of atmospheric ice-nucleating particles relevant for mixed-phase clouds. *Sci. Adv.* **6**, eaba8137 (2020).

Schill, G. P. *et al.* Widespread biomass burning smoke throughout the remote troposphere. *Nat. Geosci.* **13**, 422–427 (2020).

Tobo, Y. *et al.* Glacially sourced dust as a potentially significant source of ice nucleating particles. *Nat. Geosci.* **12**, 253–258 (2019).

Ullrich, R. *et al.* A new ice nucleation acive site parameterization for desert dust and soot. *J. Atmos. Sci.* **74**, 699–717 (2017).

Wagner, R. *et al.* Heterogeneous Ice Nucleation Ability of NaCl and Sea Salt Aerosol Particles at

Cirrus Temperatures. *J. Geophys. Res. Atmos.* **123**, 2841–2860 (2018).
Wiacek, A., Peter, T. & Lohmann, U. The potential influence of Asian and African mineral dust on ice, mixed-phase and liquid water clouds. Atmos. Chem. Phys. 10, 8649–8667 (2010).
Williamson, C. J. *et al.* A large source of cloud condensation nuclei from new particle formation in the tropics. *Nature* **574**, 399–403 (2019).
Wolf, M. J. *et al.* A biogenic secondary organic aerosol source of cirrus ice nucleating particles. *Nat. Commun.* **11**, 4834 (2020).
Yu, P. *et al.* Efficient In-Cloud Removal of Aerosols by Deep Convection. *Geophys. Res. Lett.* **46**, 1061–1069 (2019).
Zawadowicz, M. A. *et al.* Model-measurement consistency and limits of bioaerosol abundance over the continental United States. *Atmos. Chem. Phys.* **19**, 13859–13870 (2019).